Shubnikov–de Haas oscillations in the three-dimensional Dirac fermion system Ca_3PbO

Yukiko Obata,[1] Yoshimitsu Kohama,[2] Satoru Matsuishi,[3] and Hideo Hosono[1,3,*]

[1]*Laboratory for Materials and Structures, Institute of Innovative Research, Tokyo Institute of Technology, Yokohama 226–8503, Japan*

[2]*ISSP, the University of Tokyo, Kashiwa, Chiba 277–8581, Japan*

[3]*Materials Research Center for Element Strategy, Tokyo Institute of Technology, Yokohama 226–8503, Japan*

(Received 4 December 2017; revised manuscript received 17 January 2018; published 22 March 2019)

Cubic antiperovskite Ca_3PbO is a candidate for three-dimensional (3D) Dirac fermion systems that have recently emerged as a class of topological materials exhibiting linear energy dispersion in the bulk. We report magnetotransport and tunnel diode oscillation (TDO) measurements on Bi-doped Ca_3PbO in magnetic fields up to 55 T and temperatures between 2 and 78 K. By observing the Shubnikov–de Haas (SdH) oscillations, we resolve the bulk 3D Fermi surface (FS) with distinctive features of Dirac fermions including linear magnetoresistance, light effective mass, and a nontrivial phase shift. TDO measurements under high fields reveal the existence of two primary SdH frequencies, one being twice the other. Together with the low effective mass, the oscillations of these two frequencies account for the emergence of the Landau level splitting that persists up to 43 K. The field-angular-dependence of the oscillation frequencies with three branches confirms that the FS is composed of three pairs of hole pockets with uniaxial anisotropy on the Γ-X path, as predicted for bulk Ca_3PbO crystal by density functional theory calculation.

DOI: 10.1103/PhysRevB.99.115133

I. INTRODUCTION

Three-dimensional (3D) Dirac fermion systems comprise a class of topological materials where bulk conduction and valence bands with linear dispersion cross at discrete points or along curves in k space. These phenomena have been experimentally confirmed in topological semimetals incorporating those of the 3D Dirac [1–7], 3D Weyl [8–14], and topological nodal line semimetals [15,16]. Motivated by the growing interest for new Dirac materials, recent theoretical calculations on antiperovskite Ca_3PbO have predicted that there exists a 3D gapped Dirac-like cone along the Γ-X line [17], which stems from a band inversion of the Ca $3d$ and Pb $6p$ bands at the Γ point.

Following the prediction, we performed the angle-resolved photoemission spectroscopy (ARPES) experiments on Bi-doped Ca_3PbO single crystals to investigate the 3D electronic structure [18]. The ARPES and transport measurements revealed that the Bi-free samples were unintentionally heavily hole-doped so that the Fermi level (E_F) crosses not only the Dirac-like dispersion band but also the parabolic band. Thus, electron doping is necessary to assess the pure Dirac fermion system. Although the samples still remained p type even after Bi doping to Pb site, it was shown that electron doping by Bi led to the Fermi level upward shifts to the Dirac point without alternation of Dirac-like band structure [18].

In this paper, we report the magnetotransport property of Bi-doped Ca_3PbO with Shubnikov–de Haas (SdH) oscillation demonstrating the emergence of Dirac fermion system. Magnetotransport measurement is a straightforward method for detecting Dirac fermions as well as ARPES. The linear dispersion of energy band gives rise to linear quantum magnetoresistance (MR) at the quantum limit, where only the lowest Landau level (LL) crosses the E_F [19]. Another distinctive feature is the nontrivial π Berry phase shift [20], a phase generated from the cyclotron motion of electrons along a Dirac point. These characteristics have been widely confirmed in such Dirac materials as graphene [21,22], topological insulators [23–25], and topological semimetals [4,5,26–31].

For Bi-doped Ca_3PbO, we observed a linear MR at temperatures up to 40 K. The SdH oscillations are clearly discerned at low temperatures and reveal a nontrivial phase shift, complementary to previous ARPES measurements. Owing to the low effective mass and the existence of two SdH frequencies, one being twice the other, the LL splitting was observed at temperatures as high as 43 K. The field-angular dependence of SdH frequencies in high magnetic field shows at least three branches corresponding to three pairs of uniaxial FS pockets on the Γ-X path reflecting the cubic symmetry of bulk crystal.

II. EXPERIMENTAL DETAILS

Single crystals of $Ca_3(Pb_{1-x}Bi_x)O$ were grown by using Ca as a flux, as described in Refs. [18,32]. To reduce the evaporation loss from a Ca melt in an iron crucible during the growth process, the crucible was sealed in a stainless steel capsule in which two short stainless steel rods were placed at top and bottom sides of crucible to reduce open space. Due to the suppression of Ca deficiency, the hole carrier density N in the grown crystal was decreased down to $\sim 2.0 \times 10^{19}\,\mathrm{cm}^{-3}$ at 2 K, which is about 1/3 of that in the previous study [18]. The compositional formula of Bi-doped Ca_3PbO single crystals was determined to be $Ca_{2.92(9)}Pb_{0.98(3)}\ Bi_{0.015(2)}O_{1.3(4)}$ by electron-probe microanalysis, showing that the crystals still contain vacancies on approximately 2% of the Ca sites.

Magnetotransport measurements were performed in the standard Hall and resistivity configuration using a Quantum

*Corresponding author: hosono@msl.titech.ac.jp

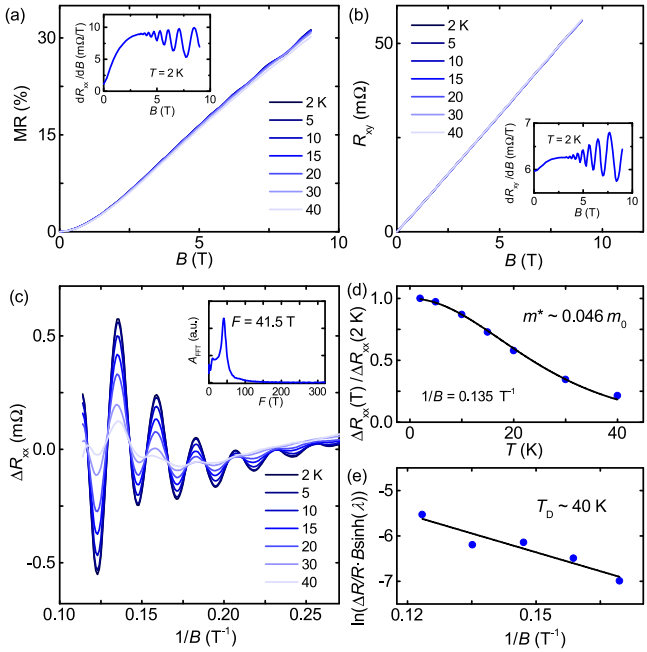

FIG. 1. SdH oscillations under dc fields and Fermi surface parameters. (a),(b) MR and R_{xy} vs B for Bi-doped Ca_3PbO up to 9 T at temperatures between 2 and 40 K. The insets show the derivatives dR_{xx}/dB and dR_{xy}/dB vs B at 2 K, respectively. (c) Oscillatory component of longitudinal resistivity ΔR_{xx} vs $1/B$ at various temperatures. The inset shows the FFT spectrum of the SdH oscillations at 2 K. (d) Oscillation amplitudes $\Delta R_{xx}(T)/\Delta R_{xx}$ (2 K) vs T for the peak at $1/B = 0.135\,\mathrm{T}^{-1}$. (e) Dingle plot of the SdH oscillations with the oscillation frequency $F = 41.5\,\mathrm{T}$.

Design 9T–Physical Property Measurement System (PPMS). Crystals were fixed on sapphire substrates by applying Stycast 2850 epoxy and contacted using silver epoxy in an argon glovebox to avoid exposure to an ambient atmosphere, and were then immersed in Paratone-N oil before transferring the sample to the measurement chamber in PPMS. Quantum oscillations measurements with a tunnel diode oscillator technique (TDO) [33] were also conducted by attaching the samples to a copper coil of ~8 turns that comprises part of a TDO circuit, resonating at ~82 MHz. The sample with coil was rotated *in situ*, θ being the angle between the magnetic flux density $\boldsymbol{B}$ and the [001] direction. Magnetic fields ($\mu_0 H$) of up to 55 T were applied by the nondestructive pulse magnet at the Institute for Solid State Physics, the University of Tokyo. The magnetization of the sample is neglected in the following sections ($B = \mu_0 H$).

To provide a theoretical reference with which to compare our magnetotransport results, we performed density functional theory (DFT) band structure calculations with the Perdew-Burke-Ernzerhof generalized-gradient approximation [34] using the VASP code [35], while the effective mass and hole carrier concentration were calculated using the SKEAF code [36].

III. LINEAR MAGNETORESISTANCE

Figure 1(a) shows the MR ratio (%) $[\rho(B) - \rho(0)]/\rho(0) \times 100$ as a function of B up to 9 T at temperatures between 2 and 40 K with a field applied along the c axis (i.e., $B \perp ab$ plane). While the derivative of the longitudinal resistance dR_{xx}/dB [inset in Fig. 1(a)] linearly increases in the low B region, it is saturated in the high B region and oscillates along a straight line. This result indicates the transition from the semiclassical B^2 dependent to the linear B-dependent MR, which is consistent with the behavior observed in such Dirac materials as $Ba(FeAs)_2$ [37]. SdH oscillations can be resolved from as low as $B = 5\,\mathrm{T}$ in both MR and Hall resistance R_{xy} with the help of the derivatives dR_{xx}/dB and dR_{xy}/dB, as shown in Figs. 1(a) and 1(b), respectively.

IV. QUANTUM OSCILLATIONS IN DC FIELDS

A. Frequency and effective mass

By subtracting a polynomial background of R_{xx} at $2\,\mathrm{K} < T < 40\,\mathrm{K}$, SdH oscillations periodic in $1/B$ are observed [Fig. 1(c)]. The fast Fourier transform (FFT) spectrum of the SdH oscillations as a function of B at 2 K [see the inset in Fig. 1(c)] reveals a single oscillation frequency $F = 41.5\,\mathrm{T}$, which corresponds to the periodicity $\Delta(1/B) = 0.024\,\mathrm{T}^{-1}$. According to the Onsager relation, $F = (\hbar/2\pi e)S_F$, where $\hbar$ is Planck's constant and S_F is a cross-sectional area of FS normal to the field, we obtain $S_F = 3.9 \times 10^{-3}\,\mathrm{\AA}^{-2}$, a tiny area corresponding to only 0.2% of the cross-sectional area of the first Brillouin zone (BZ). By assuming a circular cross section, a very small Fermi wave vector of $k_F = 0.035\,\mathrm{\AA}^{-1}$ is estimated.

Quantum oscillation of resistance ΔR_{xx} can be described by Lifshitz-Kosevich (LK) formula [38,39]:

$$\frac{\Delta R_{xx}}{\Delta R_{xx}(0)} = C\sum_{p=1}^{\infty} R_T R_D R_s \frac{1}{\sqrt{p}} \cos\left[2\pi p\left(\frac{F}{B} - \frac{1}{2} + \phi_D + \phi_B\right)\right], \tag{1}$$

where $\Delta R_{xx}(0)$ is the background resistivity, C is a positive coefficient, and p represents the pth harmonic oscillation. The temperature and Dingle factors are expressed as $R_T = \lambda(T)/\sinh(\lambda(T))$ and $R_D = e^{-\lambda_D}$ with $\lambda_{(D)} = 2\pi^2 p k_B T_{(D)} m^*/(\hbar e B)$, where k_B and m^* represent the Boltzmann constant and the effective cyclotron mass. The spin damping factor is given by $R_S = \cos(p\pi \frac{g}{2}\mu^*)$, where $\mu^* = m^*/m_0$ with m_0 being the bare electron mass, and g represents the spin g factor. The phase factor ϕ_D is determined by the dimensionality of the FS, and the value varies from 0 for 2D FS to + or −1/8 for a minimum or maximum cross section of 3D FS, respectively [38,39]. Another phase factor ϕ_B is the Berry phase, which is 0 for normal electrons but 1/2 for Dirac fermions [20]. Due to the maximum cross section of the 3D FS, the total phase shift, given by $\phi = \phi_D + \phi_B$, for Ca_3PbO is expected to be 3/8.

Figure 1(d) shows the temperature dependence of the relative oscillatory component $\Delta R_{xx}(T)/\Delta R_{xx}(2\,\mathrm{K})$ for the peak at $1/B = 0.135\,T^{-1}$. For simplicity, we have neglected harmonics here. The fit yields $m^* \sim 0.046\,m_0$. Subsequently, the Fermi velocity $v_F = \hbar k_F/m^*$ is calculated to be $v_F = 8.77 \times 10^5\,\mathrm{m/s}$. A long mean free path of $l_q = 26\,\mathrm{nm}$ can be derived from the Dingle temperature $T_D \sim 40\,\mathrm{K}$ obtained from the Dingle plot [Fig. 1(e)]. The quantum

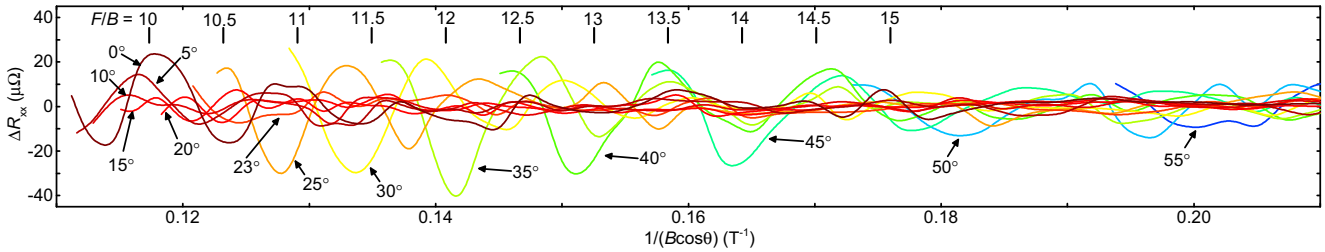

FIG. 2. Oscillatory components of the resistance as a function of $1/(B\cos\theta)$ at various angles, measured for another sample with $m^*(0) \sim 0.074\, m_0$.

mobility μ_q calculated by $\mu_q = e\tau_q/m^*$ is $1132\,\mathrm{cm^2\,V^{-1}\,s^{-1}}$. The values of these band parameters are comparable to those of well-studied 3D Dirac fermion systems such as Cd_3As_2 [5,40].

B. Lande *g* factor and Berry phase

Next, we consider the spin damping factor R_S and oscillation phases. For the analysis of the g factor, the spin-zero method has been widely used in quantum oscillation studies on 2D or quasi-2D materials such as organic metals [41], high-T_c cuprates [42,43], and iron-based superconductors [44]. The cross-sectional area of FS in a quasi-2D metal increases as a function of $1/\cos\theta$ while tilting the field, leading to an increase in cyclotron mass, $\mu^*(\theta) = \mu^*(0)/\cos\theta$. Substitution of this θ dependence in the equation of R_S results in a periodic disappearance of R_S with the spin-zero condition for the fundamental harmonic, $g\mu^*(\theta) = 2n + 1$, where n is an integer [41]. Thus, to determine the values of the two unknowns, $g\mu^*(\theta)$ and n, at least two successive spin-zero angles need to be detected.

Figure 2 shows the oscillatory components of the resistance as a function of $1/(B\cos\theta)$ at various angles of the magnetic field with respect to the normal of the sample surface, measured for another sample with $m^*(0) \sim 0.074\, m_0$. The curves at $\theta = 0°$ and 5° show a maximum near $F/B = 11$, while that at $\theta = 25°$ shows a minimum, suggesting that the first spin-zero exists between $\theta = 0°$ and 25°. Likewise, the second spin-zero can be identified between $\theta = 25°$ and 45° near $F/B = 13.5$. Furthermore, by looking at the curves near $F/B = 14.5$, we can see that the waveform at $\theta = 45°$ almost remains the same until $\theta = 50°$, whereas it is hard to distinguish the curve at $\theta = 55°$.

Under an assumption that the first spin-zero is at $\theta = 15 \pm 5°$ with $\mu^* = 0.076$, we can obtain a g factor, $g = 13.12(2n + 1)$. If we take $n = 2$ ($g = 66(1)$), the second spin-zero emerges at $\theta = 46.4°$, which is consistent with the experimental observations. No other values for n can explain the positions and number of spin zeros detected in the experiment; that is, $n < 2$ does not account for the second spin zero, while $n > 2$ yields extra spin zeros. With $g = 66(1)$ and $\mu^* = 0.046$ at $\theta = 0°$, the phase of R_S for the oscillations shown in Fig. 1(c), $\pi\frac{g}{2}\mu^*$, is estimated to be 1.52π and hence $R_S > 0$. This considerably large g factor suggests the existence of strong spin-orbit coupling in Ca_3PbO, which is predicted to account for the band inversion at Γ leading to the emergence of 3D Dirac fermions in Ca_3PbO.

We now evaluate the phase shift ϕ for Ca_3PbO. The nontrivial π Berry phase has been recognized as a hallmark of various Dirac materials [5,22,23,31], and ϕ can be determined either directly from the fit to the LK formula or the LLindex plot. Figure 3(a) shows the oscillatory component of magnetoconductivity $\sigma_{xx}(B)$ of the sample (characterized by Fig. 1) as a function of $1/B$ at 2 K, obtained by using the formula $\sigma_{xx}(B) = \rho_{xx}/(\rho_{xx}^2 + \rho_{xy}^2)$, where ρ_{xx} and ρ_{xy} are the longitudinal and Hall resistivities, respectively. The LK fit of $\Delta\sigma_{xx}$ yields the phase shift of $\phi = 0.376(3)$, which is closely equivalent to the value predicted for Ca_3PbO. In addition, to perform the LL index plot, we assign LL integer indices n to minima in $\Delta\sigma_{xx}$ and half indices to maxima in $\Delta\sigma_{xx}$ [45], shown in Fig. 3(b). In case of $R_S > 0$, the nth minimum in $\Delta\sigma_{xx}$ satisfies the following relation [46]:

$$2\pi\left(\frac{F}{B} - \frac{1}{2} + \phi\right) = (2n - 1)\pi. \tag{2}$$

Thus, the plot of n vs $1/B$ makes a straight line with F and ϕ, which correspond to the slope and intercept on the n axis, respectively. The best-fit straight line in Fig. 3(b) intercepts the n axis at the value $\phi = 0.36(5)$, consistent with the value derived from the LK fit. However, in a recent theoretical work, it is argued that the phase shift ϕ in the fundamental oscillation should not be interpreted as direct evidence for 3D Dirac fermions, emphasizing that it represents a phase defined by spin-orbit coupling constant λ, further accounting for the Zeeman contribution [47]. With this definition, further theoretical studies are required to evaluate the phase shift expected for Ca_3PbO.

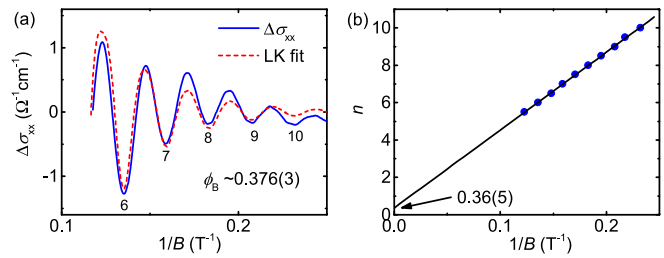

FIG. 3. (a) Oscillatory component of magnetoconductivity of the Bi-doped Ca_3PbO single crystal, characterized by transport properties shown in Fig. 1, $\Delta\sigma_{xx}$ vs $1/B$ fitted to the LK formula. The minima positions are assigned as integer LL indices. (b) LL index plot.

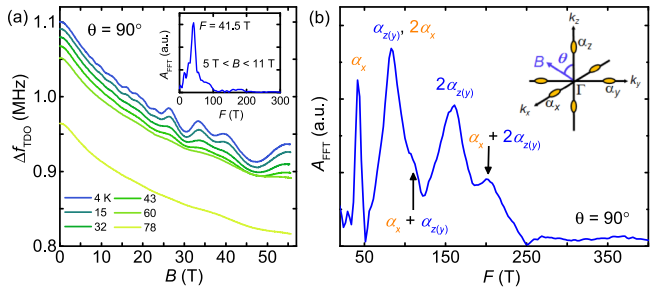

FIG. 4. High magnetic field data obtained from TDO measurements. (a) Resonant frequency, Δf_{TDO}, vs B up to 55 T at temperatures between 4 and 78 K with the field applied normal to the (001) plane. The inset shows the FFT spectrum of the SdH oscillations at 4 K for fields between 5 and 11 T. (b) FFT spectra of oscillatory component $\Delta f_{\mathrm{TDO}}^{\mathrm{OSC}}$ at 4 K. The peaks are assigned as α_x and α_z with their second harmonics and their combinations. The inset shows the schematic image of the ellipsoidal FS in the 3D BZ of Ca_3PbO.

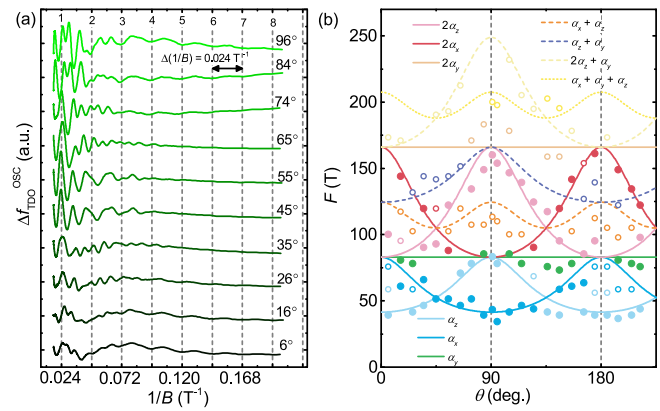

FIG. 5. Angular dependence of SdH oscillations under high magnetic fields. (a) Oscillatory component $\Delta f_{\mathrm{TDO}}^{\mathrm{OSC}}$ at various angles. (b) Angular dependence of the FFT peak positions. The solid and dashed lines show the simulated results for the 3D ellipsoidal model using harmonics and combinations, respectively. The solid and open dots represent the FFT peaks with high and low amplitudes.

V. QUANTUM OSCILLATIONS IN HIGH FIELDS

A. Zeeman splitting

To investigate the quantum limit of the SdH oscillations in high fields, we performed TDO measurements instead of using the standard four-probe configuration method, which was unfeasible for our samples due to the difficulty of making stable contacts for the measurements in pulse magnetic fields. Figure 4(a) shows the field dependence of the resonant frequency up to 55 T at temperatures between 4 and 78 K with the field applied normal to the (001) plane. The frequency variation Δf_{TDO} represents the change in the conductance of the sample following the relation, $\Delta f_{\mathrm{TDO}} \propto 1/\rho_{xx}$, where ρ_{xx} is the longitudinal resistivity.

To conduct background subtraction, we use the linear interpolation of the raw data at 78 K. The FFT spectrum [inset in Fig. 4(a)] of the oscillatory component $\Delta f_{\mathrm{TDO}}^{\mathrm{OSC}}$ at 4 K in the low-field range ($5\,\mathrm{T} < B < 11\,\mathrm{T}$) reveals a single oscillation frequency $F = 41.5\,\mathrm{T}$, consistent with the results of the four-probe configuration measurements in DC magnetic fields. In contrast, $\Delta f_{\mathrm{TDO}}^{\mathrm{OSC}}$ at 4 K [blue line in Fig. 4(a)] in the high-field range ($3\,\mathrm{T} < B < 55\,\mathrm{T}$) shows oscillations with multiple frequencies, which appear as additional peaks other than the peak at $F = 41.5\,\mathrm{T}$ in the FFT spectrum [Fig. 4(b)]. Regarding the origins of these extra peaks, we consider two candidates: other extremal orbits due to anisotropy of the Fermi surfaces and harmonics generation by Zeeman splitting.

Our DFT calculation predicts that the bulk Fermi surface of slightly hole-doped Ca_3PbO forms three pairs of nearly ellipsoidal hole pockets on Γ-X lines, α_x, α_y, and α_z, which can be transferred to each other by cubic crystal symmetry [17]. The inset in Fig. 4(b) depicts the schematic image of α_x, α_y, and α_z in the 3D BZ of Ca_3PbO. Actually, our previous ARPES measurement demonstrated the existence of hole pockets on Γ-X lines and the distinct Fermi velocities along the two cuts crossing either a single or double Dirac point [18]. In particular, the DFT calculation shows that the cross-sectional area of α_z is approximately twice as large as that of α_x when the field applied along the k_x axis [$\theta = 90°$ in the inset shown in Fig. 4(b)]. In this case, as the angle between the field and the [001] direction increases, the oscillation with $F = 41.5\,T$ (α_z) would increase and gradually approach that with $F = 83\,\mathrm{T}$, whereas the oscillation with $F = 83\,T$ (α_x) would decrease and gradually approach that with $F = 41.5\,\mathrm{T}$. As for the Zeeman splitting, the peaks in the FFT spectra would always appear twice as large as α_x and α_z.

B. Angular dependence of quantum oscillations

To verify the ellipsoidal FS model and clarify the origins of oscillation with high frequencies, we performed the angular-dependent TDO measurements by tiling the magnetic field from the [001] direction ($\theta = 0°$) to the [00-1] direction ($\theta = 180°$), which passes through the [100] ($\theta = 90°$) direction [see Fig. 4(f)]. Figure 5(a) shows the oscillatory components $\Delta f_{\mathrm{TDO}}^{\mathrm{OSC}}$ at various angles in the field range from 5 to 55 T, where the split spacing markedly changes with θ, which can be simply attributed to the angular-dependent effective mass.

Figure 5(b) shows the FFT peak positions plotted as a function of θ. The solid and open dots represent the peaks with high and low amplitudes, respectively. To confirm the dimensionality of the SdH oscillations, we use the ellipsoidal FS model parameterized by α_x, α_y, and α_z, each of them representing the oscillation frequency corresponding to the cross-sectional area of the ellipsoidal FS along the Γ-X path of the k_x, k_y, or k_z axis, respectively. As shown in the inset depicted in Fig. 4(b), while tilting the field from the [001] to the [100] direction, α_y would remain constant. On the other hand, α_x and α_z would vary with the field angle by following the equation (with a $\pi/2$ shift for α_x) [36]:

$$F(\theta) = \alpha_{x(\theta=0°)}\alpha_{z(\theta=0°)} \times \sqrt{(\cot^2\theta + 1)/\left(\alpha_{x(\theta=0°)}^2 \cot^2\theta + \alpha_{z(\theta=0°)}^2\right)}, \quad (3)$$

where $F(\theta)$, $\alpha_{x(\theta=0°)}$, and $\alpha_{z(\theta=0°)}$ represent the oscillation frequencies as a function of θ and the two primary frequencies $\alpha_x = 41.5$ and $\alpha_z = 83\,\mathrm{T}$. The ellipsoidal FS model can describe the angular dependence of the oscillation frequencies

well up to the second-order harmonics of α_x, α_y, and α_z. Most of the peaks with low amplitudes [open dots in Fig. 5(b)] can be attributed to combination frequencies of α_x, α_y, and α_z [dashed lines in Fig. 5(b)]. Some peaks with low amplitudes at $\theta = 6°$, 175°, and 185° may originate from the difference between the two frequencies of $F \sim 100$ T and 40 T.

As shown in Fig. 5(b), the angular dependence of SdH oscillations agrees well with simulated results for the ellipsoidal Fermi surface model, demonstrating the existence of multiple extremal orbits due to the anisotropic Fermi surfaces, α_x and α_z, as well as their harmonics due to Zeeman splitting, $2\alpha_x$ and $2\alpha_z$. The next question is which oscillatory amplitude is more predominant than that of the other at such angles as $\theta = 45°$ where contributions from these two origins, $\alpha_x + \alpha_z$ and $2\alpha_x$ (or $2\alpha_z$), exactly cross each other. This can be solved by looking at the adjacent angles where the oscillatory amplitude of $2\alpha_x$ (or $2\alpha_z$) is higher than that of $\alpha_x + \alpha_z$. Thus, we conclude that the high-frequency components observed at $\theta = 90°$ are dominated by harmonics of α_x and α_z oscillations. As a whole, the angular dependence of the 3D SdH oscillations provides evidence for the presence of three pairs of 3D Fermi pockets with uniaxial anisotropy along the Γ-X path in bulk Ca_3PbO, as predicted by the DFT calculation in Ref. [17].

VI. CONCLUSION

By observing the SdH oscillations, we have resolved the bulk FS of Bi-doped Ca_3PbO with distinctive features of Dirac fermions including linear magnetoresistance, low effective mass, and a nontrivial phase shift. Owing to the carriers with low effective mass and the two primary SdH frequencies, one being twice the other, the LL splitting was clearly observed at temperatures as high as 43 K. The field-angular dependence of the oscillation frequencies with three branches reveals that the FS is composed of three pairs of hole pockets with uniaxial anisotropy on the Γ-X path as predicted for bulk Ca_3PbO crystal by DFT calculation.

ACKNOWLEDGMENT

This work was supported by the Ministry of Education, Culture, Sports, Science and Technology Elements Strategy Initiative to Form Core Research Center.

[1] Z. K. Liu, J. Jiang, B. Zhou, Z. J. Wang, Y. Zhang, H. M. Weng, D. Prabhakaran, S.-K. Mo, H. Peng, P. Dudin, T. Kim, M. Hoesch, Z. Fang, X. Dai, Z. X. Shen, D. L. Feng, Z. Hussain, and Y. L. Chen, Nat. Mater. **13**, 677 (2014).

[2] M. Neupane, S.-Y. Xu, R. Sankar, N. Alidoust, G. Bian, C. Liu, I. Belopolski, T.-R. Chang, H.-T. Jeng, H. Lin, A. Bansil, F. Chou, and M. Z. Hasan, Nat. Commun. **5**, 3786 (2014).

[3] S. Borisenko, Q. Gibson, D. Evtushinsky, V. Zabolotnyy, B. Büchner, and R. J. Cava, Phys. Rev. Lett. **113**, 027603 (2014).

[4] T. Liang, Q. Gibson, M. N. Ali, M. Liu, R. J. Cava, and N. P. Ong, Nat. Mater. **14**, 280 (2015).

[5] L. P. He, X. C. Hong, J. K. Dong, J. Pan, Z. Zhang, J. Zhang, and S. Y. Li, Phys. Rev. Lett. **113**, 246402 (2014).

[6] Z. K. Liu, B. Zhou, Y. Zhang, Z. J. Wang, H. M. Weng, D. Prabhakaran, S.-K. Mo, Z. X. Shen, Z. Fang, X. Dai, Z. Hussain, and Y. L. Chen, Science **343**, 864 (2014).

[7] S.-Y. Xu, C. Liu, S. K. Kushwaha, R. Sankar, J. W. Krizan, I. Belopolski, M. Neupane, G. Bian, N. Alidoust, T.-R. Chang, H.-T. Jeng, C.-Y. Huang, W.-F. Tsai, H. Lin, P. P. Shibayev, F.-C. Chou, R. J. Cava, and M. Z. Hasan, Science **347**, 294 (2015).

[8] M. N. Ali, J. Xiong, S. Flynn, J. Tao, Q. D. Gibson, L. M. Schoop, T. Liang, N. Haldolaarachchige, M. Hirschberger, N. P. Ong, and R. J. Cava, Nature (London) **514**, 205 (2014).

[9] S.-Y. Xu, I. Belopolski, N. Alidoust, M. Neupane, G. Bian, C. Zhang, R. Sankar, G. Chang, Z. Yuan, C.-C. Lee, S.-M. Huang, H. Zheng, J. Ma, D. S. Sanchez, B. Wang, A. Bansil, F. Chou, P. P. Shibayev, H. Lin, S. Jia, and M. Z. Hasan, Science **349**, 613 (2015).

[10] B. Q. Lv, N. Xu, H. M. Weng, J. Z. Ma, P. Richard, X. C. Huang, L. X. Zhao, G. F. Chen, C. E. Matt, F. Bisti, V. N. Strocov, J. Mesot, Z. Fang, X. Dai, T. Qian, M. Shi, and H. Ding, Nat. Phys. **11**, 724 (2015).

[11] L. X. Yang, Z. K. Liu, Y. Sun, H. Peng, H. F. Yang, T. Zhang, B. Zhou, Y. Zhang, Y. F. Guo, M. Rahn, D. Prabhakaran, Z. Hussain, S.-K. Mo, C. Felser, B. Yan, and Y. L. Chen, Nat. Phys. **11**, 728 (2015).

[12] S.-Y. Xu, N. Alidoust, I. Belopolski, Z. Yuan, G. Bian, T.-R. Chang, H. Zheng, V. N. Strocov, D. S. Sanchez, G. Chang, C. Zhang, D. Mou, Y. Wu, L. Huang, C.-C. Lee, S.-M. Huang, B. Wang, A. Bansil, H.-T. Jeng, T. Neupert, A. Kaminski, H. Lin, S. Jia, and M. Zahid Hasan, Nat. Phys. **11**, 748 (2015).

[13] S.-Y. Xu, I. Belopolski, D. S. Sanchez, C. Zhang, G. Chang, C. Guo, G. Bian, Z. Yuan, H. Lu, T.-R. Chang, P. P. Shibayev, M. L. Prokopovych, N. Alidoust, H. Zheng, C.-C. Lee, S.-M. Huang, R. Sankar, F. Chou, C.-H. Hsu, H.-T. Jeng, A. Bansil, T. Neupert, V. N. Strocov, H. Lin, S. Jia, and M. Z. Hasan, Sci. Adv. **1**, e1501092 (2015).

[14] S. Souma, Z. Wang, H. Kotaka, T. Sato, K. Nakayama, Y. Tanaka, H. Kimizuka, T. Takahashi, K. Yamauchi, T. Oguchi, K. Segawa, and Y. Ando, Phys. Rev. B **93**, 161112 (2016).

[15] G. Bian, T.-R. Chang, R. Sankar, S.-Y. Xu, H. Zheng, T. Neupert, C.-K. Chiu, S.-M. Huang, G. Chang, I. Belopolski, D. S. Sanchez, M. Neupane, N. Alidoust, C. Liu, B. Wang, C.-C. Lee, H.-T. Jeng, C. Zhang, Z. Yuan, S. Jia, A. Bansil, F. Chou, H. Lin, and M. Z. Hasan, Nat. Commun. **7**, 10556 (2016).

[16] Y. Wu, L.-L. Wang, E. Mun, D. D. Johnson, D. Mou, L. Huang, Y. Lee, S. L. Bud'ko, P. C. Canfield, and A. Kaminski, Nat. Phys. **12**, 667 (2016).

[17] T. Kariyado and M. Ogata, J. Phys. Soc. Jpn. **81**, 064701 (2012).

[18] Y. Obata, R. Yukawa, K. Horiba, H. Kumigashira, Y. Toda, S. Matsuishi, and H. Hosono, Phys. Rev. B **96**, 155109 (2017).

[19] A. A. Abrikosov, Phys. Rev. B **58**, 2788 (1998).

[20] G. P. Mikitik and Y. V. Sharlai, Phys. Rev. Lett. **82**, 2147 (1999).

[21] A. L. Friedman, J. L. Tedesco, P. M. Campbell, J. C. Culbertson, E. Aifer, F. K. Perkins, R. L. Myers-Ward, J. K. Hite, C. R. Eddy, G. G. Jernigan, and D. K. Gaskill, Nano Lett. **10**, 3962 (2010).

[22] K. S. Novoselov, A. K. Geim, S. V. Morozov, D. Jiang, M. I. Katsnelson, I. V. Grigorieva, S. V. Dubonos, and A. A. Firsov, Nature (London) **438**, 197 (2005).
[23] D.-X. Qu, Y. S. Hor, J. Xiong, R. J. Cava, and N. P. Ong, Science **329**, 821 (2010).
[24] H. Tang, D. Liang, R. L. J. Qiu, and X. P. A. Gao, ACS Nano **5**, 7510 (2011).
[25] C. Shekhar, S. Ouardi, A. K. Nayak, G. H. Fecher, W. Schnelle, and C. Felser, Phys. Rev. B **86**, 155314 (2012).
[26] X. Huang, L. Zhao, Y. Long, P. Wang, D. Chen, Z. Yang, H. Liang, M. Xue, H. Weng, Z. Fang, X. Dai, and G. Chen, Phys. Rev. X **5**, 031023 (2015).
[27] C. Zhang, C. Guo, H. Lu, X. Zhang, Z. Yuan, Z. Lin, J. Wang, and S. Jia, Phys. Rev. B **92**, 041203 (2015).
[28] A. Narayanan, M. D. Watson, S. F. Blake, N. Bruyant, L. Drigo, Y. L. Chen, D. Prabhakaran, B. Yan, C. Felser, T. Kong, P. C. Canfield, and A. I. Coldea, Phys. Rev. Lett. **114**, 117201 (2015).
[29] J. Feng, Y. Pang, D. Wu, Z. Wang, H. Weng, J. Li, X. Dai, Z. Fang, Y. Shi, and L. Lu, Phys. Rev. B **92**, 081306 (2015).
[30] M. Novak, S. Sasaki, K. Segawa, and Y. Ando, Phys. Rev. B **91**, 041203 (2015).
[31] Z. Wang, Y. Zheng, Z. Shen, Y. Lu, H. Fang, F. Sheng, Y. Zhou, X. Yang, Y. Li, C. Feng, and Z.-A. Xu, Phys. Rev. B **93**, 121112 (2016).
[32] Y. Obata, S. Matsuishi, and H. Hosono, Mater. Res. Bull. **106**, 1 (2018).
[33] T. Coffey, Z. Bayindir, J. F. DeCarolis, M. Bennett, G. Esper, and C. C. Agosta, Rev. Sci. Instrum. **71**, 4600 (2000).
[34] J. P. Perdew, K. Burke, and M. Ernzerhof, Phys. Rev. Lett. **77**, 3865 (1996).
[35] G. Kresse and J. Hafner, Phys. Rev. B **47**, 558 (1993).
[36] P. M. C. Rourke and S. R. Julian, Comput. Phys. Commun. **183**, 324 (2012).
[37] K. K. Huynh, Y. Tanabe, and K. Tanigaki, Phys. Rev. Lett. **106**, 217004 (2011).
[38] D. Shoenberg, *Magnetic Oscillations in Metals* (Cambridge University Press, Cambridge, England, 1984).
[39] H. Murakawa, M. S. Bahramy, M. Tokunaga, Y. Kohama, C. Bell, Y. Kaneko, N. Nagaosa, H. Y. Hwang, and Y. Tokura, Science **342**, 1490 (2013).
[40] J. Cao, S. Liang, C. Zhang, Y. Liu, J. Huang, Z. Jin, Z.-G. Chen, Z. Wang, Q. Wang, J. Zhao, S. Li, X. Dai, J. Zou, Z. Xia, L. Li, and F. Xiu, Nat. Commun. **6**, 7779 (2015).
[41] M. V. Kartsovnik, Chem. Rev. **104**, 5737 (2004).
[42] S. E. Sebastian, N. Harrison, C. H. Mielke, R. Liang, D. A. Bonn, W. N. Hardy, and G. G. Lonzarich, Phys. Rev. Lett. **103**, 256405 (2009).
[43] S. E. Sebastian, N. Harrison, and G. G. Lonzarich, Rep. Prog. Phys. **75**, 102501 (2012).
[44] T. Terashima, H. T. Hirose, D. Graf, Y. Ma, G. Mu, T. Hu, K. Suzuki, S. Uji, and H. Ikeda, Phys. Rev. X **8**, 011014 (2018).
[45] J. Xiong, Y. Luo, Y. H. Khoo, S. Jia, R. J. Cava, and N. P. Ong, Phys. Rev. B **86**, 045314 (2012).
[46] Y. Ando, J. Phys. Soc. Jpn. **82**, 102001 (2013).
[47] A. Alexandradinata, C. Wang, W. Duan, and L. Glazman, Phys. Rev. X **8**, 011027 (2018).